Version of Record: https://www.sciencedirect.com/science/article/pii/S0266353820322119
Manuscript_d9747f44de9d094efab338041dc3f56c

Experimental assessment of Fully-Uncoupled Multi-Directional specimens for mode I delamination tests

Torquato Garulli[a,b,*], Anita Catapano[a], Daniele Fanteria[b,*], Wenyi Huang[a,c], Julien Jumel[d], Eric Martin[e]

[a] *Bordeaux INP, University of Bordeaux, Laboratoire I2M CNRS UMR 5295, Talence 33400, France*
[b] *University of Pisa, Civil and Industrial Engineering Departement, Pisa 56122, Italy*
[c] *Polytech Orléans, University of Orléans, Orléans 45100, France*
[d] *University of Bordeaux, Laboratoire I2M CNRS UMR 5295, Talence 33400, France*
[e] *Bordeaux INP, University of Bordeaux, Laboratoire LCTS, CNRS UMR 5801, Talence 33400, France*

Abstract

This paper proposes an experimental study whose goal is to validate the concept of Fully-Uncoupled Multi-Directional (FUMD) specimens for delamination tests. In order to reduce the likelihood of delamination jump, a glass/epoxy UD-fabric composite was used to fabricate double cantilever beam specimens. Mode I tests were performed with standard UD specimens and with FUMD specimens having the following delamination interfaces: 0°//0°, 0°//15°, 0°//30°, 0°//45° and -45°//45°. Delamination fronts after the tests were observed by means of ultrasonic C-scans. By comparison with the UD specimens, it is shown that FUMD sequences are able to promote a fairly symmetric and flat delamination front. Analysis of the rotations of such specimens during the test confirms that they do exhibit an uncoupled mechanical behaviour. Critical energy release rate is found to be dependent on interface plies mismatch angle, but not on global stiffness of the specimens.

Keywords: A. Laminate, B. Delamination, B. Fracture toughness, B. Interface, C. Damage Tolerance

1. Introduction

In the field of structural design, composite materials represent an appealing alternative to metals. Sectors like the aerospace and the automotive have adopted more and more these materials, due to their exceptional specific properties, that allow the design of efficient lightweight structures. In particular, long-fibres composite laminates are widely adopted in structural design, even for safety-critical components. Therefore, understanding the damage processes of laminates is of paramount importance.

Among others, delamination is one of the most critical damage modes, as it may significantly reduce mechanical properties of the structure, while being very difficult to detect. Hence, the design of safe structures demands a thorough knowledge of the delamination resistance of materials [1], typically in terms of critical strain Energy Release Rate (ERR). For these reasons, delamination has been long studied [2], and standards for evaluation of interlaminar properties of composite laminates have been developed, in particular for mode I [3], mode II [4] and mixed mode I/II [5]. For mode III, no standard

*Corresponding author. Email: daniele.fanteria@unipi.it. Address: Dipartimento di Ingegneria Civile e Industriale - Sede di Aerospaziale, Via Girolamo Caruso, 8, 56122 Pisa PI.
Email addresses: torquato.garulli@u-bordeaux.fr (Torquato Garulli), anita.catapano@bordeaux-inp.fr (Anita Catapano)

August 3, 2020

exists yet. One of the most promising solutions proposed so far is the Edge-Crack Torsion (ECT) test [6]. However, research is still ongoing [7] and mode III toughness values obtained with this test may not be accurate and reliable [8].

Despite the fact that existing standards are recommended for non-woven UD materials only (due to the limited experience gained in round robin tests), extensive experience has been collected on their use, both for UD tape and woven materials [9]. However, this concerned mostly laminates with UD stacking sequences with the main reinforcement direction parallel to the specimen longitudinal direction (0°). As a consequence, only the interface between equally oriented plies at 0° (*UD interface* hereafter) is usually characterised. Instead, applicability of standards to laminates with multidirectional (MD) stacking sequences is still questionable. The reason is that UD laminates have an uncoupled thermoelastic behaviour allowing optimal test conditions and accurate data reduction techniques. MD laminates, on the contrary, have a more complex behaviour that lead to a certain number of problems that prevent the attainment of consistent and reliable results [10]. Consequently, delamination testing of non-UD interfaces (*MD interfaces* hereafter) is a complex task. Real structures, however, are built using MD laminates, and delamination may appear at any interface.

One first issue during tests on MD laminates is the appearance of additional energy dissipation mechanisms. In standard tests involving bending of the specimen, off-axis plies may experience matrix plasticity and intralaminar damage [11]. Intralaminar damage often leads to the delamination jump (or migration) [9, 12, 13, 14, 15, 16, 17]. Strategies to model such phenomenon are currently being investigated [18, 19].

Another relevant problem with MD laminates is the presence of thermal residual stresses [20]. It was shown that such stresses may promote matrix damage and thus facilitate delamination jump [21]. Moreover, they may greatly affect the evaluation of interlaminar fracture toughness, as demonstrated by Nairn [22, 23, 24] and Yokozeki et al. [25]. The importance of thermal residual stresses depends on the laminate layup [23].

A third inconvenient is the difficulty in controlling the loading mode. When pure mode tests are performed, no other modes ERR contributions should exist. When performing mixed-mode tests, knowledge of the exact mode-mix is required, in order to meaningfully reduce and exploit experimental data. While standard delamination test procedures [3, 4, 5] are devised to address these issues for UD specimens, it is not guaranteed that the same results are achieved when using MD specimens, due to the presence of elastic couplings that modify the kinematics of the specimen and that may induce unwanted rotations and parasite modes contributions to the ERR. In such cases ERR modal contributions could be evaluated numerically [26], but not without difficulties [27].

Besides modal partition, another relevant issue concerning ERR is its distribution along the width of the delamination specimen. Common data reduction procedures for delamination tests are based on 2D theories: a straight delamination front and a uniform ERR distribution are assumed, even though this has long been proven to be an idealisation [28]. Nowadays, tools to predict delamination growth direction have been developed, following geometrical considerations [29], or within the framework of Cohesive Zone Model (CZM) [30].

It was shown that in MD laminates 3D effects can become important and affect the shape of the front and of ERR distribution [31, 32, 33, 34]. In particular, the parameter D_c [31, 32]:

$$D_c = \frac{D_{12}^2}{D_{11} D_{22}}\,, \tag{1}$$

was found to be related to curvature of ERR distribution and delamination front. Terms D_{ij} in Eq. (1) are the components of the laminate stiffness matrix, as obtained by Classical Laminated Plate Theory (CLPT). On the other hand, the asymmetry of ERR distribution and of delamination front was found to be somewhat related to the parameter B_t [33, 34]:

$$B_t = \left| \frac{D_{16}}{D_{11}} \right| . \tag{2}$$

In order to obtain reliable evaluations of critical ERR using common data reduction techniques, both D_c and B_t should be kept as small as possible [35]. According to [36], the value of D_c should be much lower than 1, while in [37] it was suggested that it be lower than 0.25 (referring however to End Notched Flexure specimens).

To sum up, delamination testing of MD interfaces requires an extremely careful design of the stacking sequence for the specimens. As observed in [38, 39], the ideal stacking sequence should result in specimens that avoid as much as possible additional damage mechanism, that eliminate (or at least reduce) mechanical couplings, and that are not affected by thermal residual stresses. One approach suggested is to use stacking sequences containing as much 0°-oriented plies as possible [12, 33]. This approach reduces, but does not eliminate, couplings and thermal stresses. Other authors used FE simulations to try and find suitable stacking sequences [16, 21]. Eventually some authors adopted an innovative approach by using quasi-trivial (QT) solutions [40] to obtain uncoupled specimens [41, 42, 43]. While only specific sequences were developed (thus with limitations on possible interfaces and on the capability to investigate other aspects), this novel approach allowed to build specimens with interesting uncoupling properties.

This same approach was pushed further in a previous work [44], where the authors presented a method based on QT solutions and special superposition rules [45, 46] to conceptually design novel Fully-Uncoupled Multi-Directional (FUMD) stacking sequences. This design approach aims at generating layups for delamination specimens that are not affected by thermal residual stresses, do not have any elastic coupling, and allow to test any desired delamination interface. Such results were obtained in closed-form solution within the framework of CLPT and verified by means of Finite Element analyses in [44]. This preliminary assessment suggested that FUMD specimens could represent an extremely appealing solution for delamination testing of MD interfaces.

To confirm such approach, this paper shows the results of the very first experimental campaign carried out using FUMD sequences and taking into account different delamination interfaces and different global stiffness properties of the specimens. The main goal of such activity was to experimentally assess the capability of FUMD sequences to deliver uncoupled behaviour, to produce the expected delamination fronts, to avoid undesired rotations and to allow an easy evaluation of the critical ERR with simple procedures proposed by standards.

The paper is organised as follows. Firstly, Section 2 recalls the fundamentals of FUMD stacking sequences and explains in detail how they were used to design the delamination specimens conceived

for this study. Then, the material system and all the experimental procedures adopted, from specimen fabrication to data reduction, are described. Section 4 presents and discusses the results of the study. Eventually Section 5 ends the paper with conclusions and perspectives.

2. Delamination specimens design

The theoretical principles behind the design of FUMD stacking sequences for delamination specimens have been presented for the first time in a previous work from the authors [44]. Hence, only those notions fundamental for the understanding of the present paper will be reported here. On the other hand, some more details on how to practically obtain a FUMD specimen will be given.

2.1. Classic laminated plate theory and quasi-trivial solutions

The mechanical behaviour of a composite laminate, Fig. 1, may be described using the CLPT, which gives the constitutive relationship between generalised forces, $\mathbf{N}$ and $\mathbf{M}$, and generalised strains, $\boldsymbol{\epsilon}_0$ and $\boldsymbol{\chi}$, of the middle plane:

$$\begin{Bmatrix} \mathbf{N} \\ \mathbf{M} \end{Bmatrix} = \begin{bmatrix} \mathbf{A} & \mathbf{B} \\ \mathbf{B} & \mathbf{D} \end{bmatrix} \begin{Bmatrix} \boldsymbol{\epsilon}^0 \\ \boldsymbol{\chi} \end{Bmatrix} - T \begin{Bmatrix} \mathbf{U} \\ \mathbf{V} \end{Bmatrix}, \tag{3}$$

In Eq. (3), T is the actual temperature, evaluated with respect to that of a reference unstrained condition. $\mathbf{A}$, $\mathbf{B}$ and $\mathbf{D}$ are the membrane, membrane/bending coupling and bending stiffness matrices, respectively; vectors $\mathbf{U}$ and $\mathbf{V}$ express in-plane forces and moments caused by thermal effects, respectively.

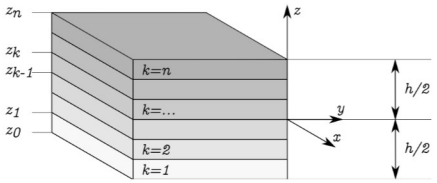

Figure 1: Laminate stacking parameters and notation.

For convenience, normalised stiffness and thermal matrices are defined as follows:

$$\mathbf{A}^* = \frac{\mathbf{A}}{h}, \quad \mathbf{B}^* = 2\frac{\mathbf{B}}{h^2}, \quad \mathbf{D}^* = 12\frac{\mathbf{D}}{h^3}, \quad \mathbf{U}^* = \frac{\mathbf{U}}{h}, \quad \mathbf{V}^* = 2\frac{\mathbf{V}}{h^2}. \tag{4}$$

A laminate is said to be *uncoupled* if:

$$\mathbf{B} = \mathbf{0}, \tag{5}$$

while it is called *quasi-homogeneous* if, along with Eq. (5), it also has:

$$\mathbf{A}^* = \mathbf{D}^*. \tag{6}$$

A UD laminate represents a very special case, as it yields:

1. $\mathbf{B} = \mathbf{0}$;
2. $\mathbf{A}^* = \mathbf{D}^*$;

3. $A_{16} = A_{26} = D_{16} = D_{26} = 0$;
4. $\mathbf{V} = \mathbf{0}$;
5. $U_{xy} = 0$;

In the case of a UD delamination specimen, the entire specimen and both its arms satisfy the above conditions. In addition, the normalised stiffness and thermal matrices of the entire specimen and of its arms are identical.

Vannucci and Verchery demonstrated the existence of a particular class of closed-form analytical solutions to Eqs. (5) and (6), which they called quasi-trivial [40]. These solutions are defined in terms of how plies' orientations are distributed within the sequence, but do not depend on the values of orientations themselves. Hence, such values can be chosen freely to satisfy further requirements. Moreover, for QT uncoupled solutions also the vector of thermally-induced moments acting on the laminate is identically null , $\mathbf{V} = \mathbf{0}$ [40].

2.2. FUMD stacking sequences: fundamentals

FUMD stacking sequences have been developed to solve the long-standing problem of finding appropriate layups for multi-directional delamination specimens. Indeed, using such sequences, it is possible:

1. to test any type of delamination interface;
2. to prevent thermal residual stresses;
3. to design specimens whose mechanical behaviour mimics that of UD ones: no mechanical coupling exists, both in the entire specimen and in its arms considered separately.

To obtain a FUMD sequence, the sequences composing each arm of the delamination specimen have to be QT quasi-homogeneous solutions. This guarantees that $\mathbf{B} = \mathbf{0}$, $\mathbf{A}^* = \mathbf{D}^*$ and that no thermally-induced moments will act on the laminate ($\mathbf{V} = \mathbf{0}$). Secondly, they have to be chosen such that shear-extension and bending-torsion couplings are eliminated as well (i.e. the laminate is specially orthotropic [47], $A_{16} = A_{26} = D_{16} = D_{26} = 0$). To do this, a balanced laminate may be used: this eliminates the shear-extension coupling and, by virtue of quasi-homogeneity, the bending-torsion coupling too. It is possible to demonstrate that the use of a balanced laminate also eliminates the thermally-induced shear on the laminate ($U_{xy} = 0$) [44]. Consequently, the behaviour of each specimen arm is macroscopically identical (in terms of thermo-mechanical couplings) to that of a UD laminate. Eventually, the sequences adopted for the two arms must comply to superposition rules for QT solutions that were derived in [46]. For the particular case at hand, the two sequences should have the same number of plies for each given orientation. If also this last condition is met, a FUMD stacking sequence is obtained, that is: the layup of the entire specimen, which results from the superposition of the two layups forming its arms, will show the same macroscopic properties as those of each arm.

2.3. FUMD specimens design

For this study, five types of FUMD specimens for mode I delamination were designed and fabricated.

The first step is the selection of appropriate QT quasi-homogeneous layups from the database of QT solutions, [46]. The following sequences were selected:

$$QT_1 = [\theta\,/\,\alpha\,/\,\beta\,/\,\beta\,/\,\theta\,/\,\alpha\,/\,\theta\,/\,\theta\,/\,\alpha\,/\,\theta\,/\,\beta\,/\,\beta\,/\,\alpha\,/\,\theta]\,,$$
$$QT_2 = [\alpha\,/\,\theta\,/\,\beta\,/\,\theta\,/\,\theta\,/\,\beta\,/\,\beta\,/\,\alpha\,/\,\alpha\,/\,\theta\,/\,\theta\,/\,\alpha\,/\,\theta\,/\,\beta]\,.$$

As a first remark, being QT solutions, they are defined as sequences of generic orientations (α, β and θ). From a practical point of view, these sequences have been chosen for the following reasons:

1. they present useful similarities: three orientations, allocated in the same manner. Therefore, they can be made compliant to the superposition rules for QT solutions mentioned in Section 2.2;
2. they both allow a balanced laminate, if the θ orientation is aligned to one in-plane reference axis (0° or 90°) and the other two orientations are taken as opposites. So choosing $\theta = 0°$ and $\beta = -\alpha$ allows to eliminate shear-extension and bending-torsion couplings, and thermally-induced shear as well;
3. the sequences have different orientations for their outermost plies, allowing to be combined in different ways and thus obtain different delamination interfaces.

With the above conditions applied, the two sequences reduce to:

$$QT_1 = [0\,/\,\alpha\,/\,-\alpha\,/\,-\alpha\,/\,0\,/\,\alpha\,/\,0\,/\,0\,/\,\alpha\,/\,0\,/\,-\alpha\,/\,-\alpha\,/\,\alpha\,/\,0]\,,$$
$$QT_2 = [\alpha\,/\,0\,/\,-\alpha\,/\,0\,/\,0\,/\,-\alpha\,/\,-\alpha\,/\,\alpha\,/\,\alpha\,/\,0\,/\,0\,/\,\alpha\,/\,0\,/\,-\alpha]\,.$$

All the FUMD sequences selected for this study are reported in Table 1, each with an identifying label highlighting the delamination interface. Standard UD delamination specimens are also included. In more detail:

1. sequences FUMD 0//15, FUMD 0//30 and FUMD 0//45 are obtained superposing sequence QT_2 to QT_1, and then choosing $\alpha = 15°$, 30° and 45° respectively;
2. sequence FUMD 0//0 is obtained superposing sequence QT_1 to itself and choosing $\alpha = 45°$;
3. sequence FUMD -45//45 is obtained superposing sequence QT_2 to itself and choosing $\alpha = 45°$.

Sequences FUMD 0//15, FUMD 0//30 and FUMD 0//45 are used to evaluate effects of the mis-orientation on fracture toughness of the interface. Delamination interfaces of the type 0//θ in mode I delamination were studied both with numerical tools [21, 48] and experimentally [16, 49, 50, 51, 52, 53]. It is worth mentioning that these sequences have, of course, different global stiffness matrices, as obtained according to CLPT. As reported by some authors [43], this might influence fracture toughness.

On the other hand, sequences FUMD 0//0 and FUMD -45//45 were designed to have exactly the same global stiffness as FUMD 0//45, but different interfaces. Therefore, if differences are observed in the fracture toughness obtained with these three sequences, they cannot derive from differences in global stiffness. On the contrary, they may result from local effects, like the orientations of plies embedding the delamination interface, and of adjacent plies at most. Relevant mode I studies on delamination interfaces of the type -θ//θ may be found in [13, 16, 17, 21, 41, 48, 51].

Label	Stacking sequence	D_c
UD	$[0_{14}//0_{14}]$	0.025
FUMD 0//15	[0 / 15 / -15 / -15 / 0 /15 / 0 / 0 / 15 / 0 / -15 / -15 / 15 / 0 // 15/0 / -15 / 0 / 0 / -15 / -15 / 15 / 15 / 0 / 0 / 15 / 0 / -15]	0.041
FUMD 0//30	[0 / 30 / -30 / -30 / 0 / 30 / 0 / 0 / 30 / 0 / -30 / -30 / 30 / 0 // 30 / 0 / -30 / 0 / 0 / -30 / -30 / 30 / 30 / 0 / 0 / 30 / 0 / -30]	0.085
FUMD 0//45	[0 / 45 / -45 / -45 / 0 / 45 / 0 / 0 / 45 / 0 / -45 / -45 / 45 / 0 // 45 / 0 / -45 / 0 / 0 / -45 / -45 / 45 / 45 / 0 / 0 / 45 / 0 / -45]	0.110
FUMD 0//0	[0 / 45 / -45 / -45 / 0 / 45 / 0 / 0 / 45 / 0 / -45 / -45 / 45 / 0 // 0 / 45 / -45 / -45 / 0 / 45 / 0 / 0 / 45 / 0 / -45 / -45 / 45 / 0]	0.110
FUMD -45//45	[45 / 0 / -45 / 0 / 0 / -45 / -45 / 45 / 45 / 0 / 0 / 45 / 0 / -45 // 45 / 0 / -45 / 0 / 0 / -45 / -45 / 45 / 45 / 0 / 0 / 45 / 0 / -45]	0.110

Table 1: Stacking sequences used for the study, associated labels and values of the parameter D_c obtained using material properties of Table 2. The double slash indicates mid-plane (delamination) interface.

Finally, sequence FUMD 0//0 has the same interface as the standard UD one, but significantly different global stiffness. Hence, results obtained with such sequences may be compared to observe possible effects of stiffness on critical ERR.

3. Delamination specimens fabrication and testing procedure

3.1. Material system adopted

The material system used for this study is a glass-epoxy *UD-fabric*, with 90% of fibre weight in the longitudinal direction (0°, warp) and the remaining 10% in the transverse direction (90°, weft). Its commercial reference is: HexPly © M34N/32%/ 430PUD/G-136x5 and it was available in the form of a prepreg. Since FUMD specimens do not address directly the problem of delamination jump, this material was used to mitigate the problem. Indeed, Ozdil et al. [54, 55, 56] used a similar material to perform delamination tests on MD specimens and reported that no delamination migration was observed. Recently, a UD-fabric composite was used fro the same purpose by Gong et al. [41].

It should be remarked that delamination in woven composites presents some differences with respect to UD materials [57]. Firstly, fibre bridging is rarely observed in woven composites, contrarily to UD ones. Studies confirmed its absence in four-harness satin woven glass/vinylester [58] and in five-harness satin weave carbon/epoxy [59] composites. Others reported evidence of fibre bridging only for some weave patterns tested [60, 61]. Other differences lay in the fracture process, that in woven composites is more complex and is influenced by both the weave pattern [58, 59, 60, 61, 62] and the orientation of layers embedding the delamination [41, 56, 59, 60]. These aspects influence the micro-structure at the interface level and have an effect on the thickness of the interply resin region [58] and on the undulation of the fracture surfaces [58, 63]. This, in turn, influences the fracture toughness of the composite. In some cases the weave pattern was found to affect fracture toughness more than fibre type [62].

Elastic properties of the material were obtained with a dedicated experimental characterisation campaign based on ASTM standards [64, 65, 66]. Table 2 reports the results obtained along with their percent coefficient of variation.

	$E_{1,t}$ [GPa]	$E_{1,f}$ [GPa]	$E_{2,t}$ [GPa]	$E_{2,f}$ [GPa]	G_{12} [GPa]	ν_{12} [-]
Average	40.5	39.0	17.4	15.8	6.16	0.248
Std. Dev.	0.75	1.03	0.28	0.48	0.13	$4.3{\cdot}10^{-3}$
C. Var. %	1.84	2.63	1.61	2.95	2.15	1.74

Table 2: Elastic properties of the UD-fabric material adopted, obtained by experimental characterisation.

3.2. Fabrication

The prepreg material was cut in rectangular patches with a numerically-controlled machine, at any desired orientation with respect to the warp direction. The lay-up process was performed manually. A 25 μm thick Fluorinated Ethylene Propylene (FEP) insert film (Aerovac A5000) was used as a delamination starter. Following the indications of the pre-preg manufacturer, the plates were cured in an autoclave at 75° C and a pressure of 3 bars for 8 hours. No post-cure was performed. From each plate, seven Double Cantilever Beam (DCB) specimens 25 mm wide and 200 mm long were obtained, by means of water-jet cutting. The insert length within the specimens was of about 63 mm, resulting in an initial delamination length (measured from the insert tip to the load line) of about 50 mm.

3.3. Experimental procedure

All specimens were labelled and measured. The insert length was measured with the aid of an optical microscope. Compliance with dimensional requirements suggested in [3] was verified. All UD specimens and five FUMD ones of each type (# 2, 3, 5, 6, 7) had one side white painted and marked at regular interval, to keep track of delamination, Fig. 2. End blocks were installed on both specimen arms. Specimens were not conditioned before tests, that were carried out at room temperature (23.0 ± 0.6°C).

Mode I delamination tests were performed with the setup shown in Fig.3. A double actuator system with the specimen in vertical position was used. This innovative solution allows to obtain optimal test conditions: gravity does not affect symmetry of the configuration and the double actuation ensures symmetry of the applied boundary conditions. According to [3], each specimen was firstly loaded up to the beginning of delamination propagation, and until delamination, as visually observed, propagated 3-6 millimetres; then the specimen was unloaded. Afterwards, the specimen was loaded again, until delamination propagated up to about 50 mm from the initial insert tip position. A constant opening displacement rate of 1 mm/min was used during both loading phases. Along with force and displacements, the load points rotations were recorded, by means of inclinometers, see Fig. 3; sampling rate was 10 Hz for all these quantities. Two cameras (Canon EOS 800D and Canon EOS 750D) regularly and automatically took pictures (at a resolution of 6000×4000 pixels) of the specimen: on one side, a global view of the

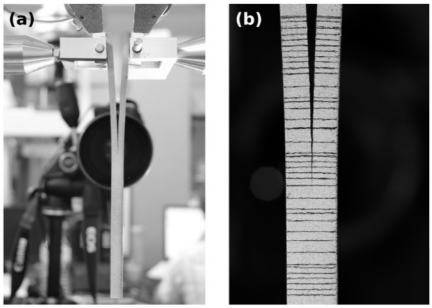

Figure 2: Sample pictures taken during the tests: global view of the specimen (a) and zoom on the propagation region (b).

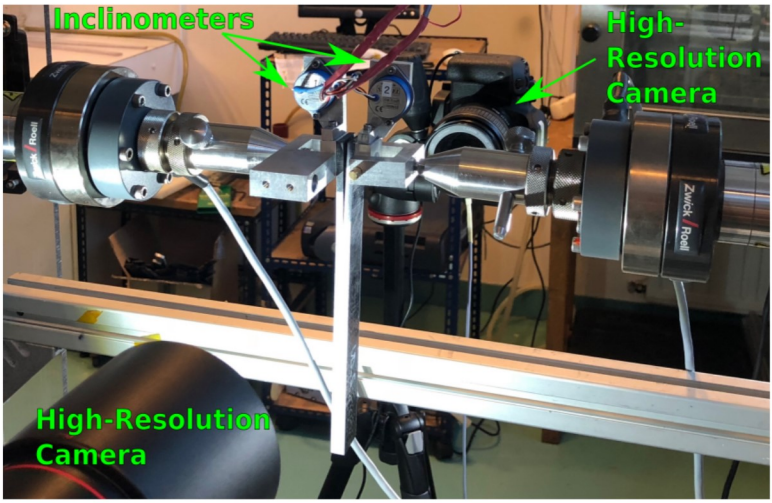

Figure 3: View of the experimental set-up used for mode I delamination tests.

specimen was caught, while on the other one a close zoom in the propagation region was set, Fig. 2. At the exact instants at which pictures were taken, load, displacements and load points rotations were recorded.

After the tests, all specimens were observed by means of ultrasonic C-scans, performed manually with an Olympus OmniScan SX device [67, 68, 69], coupled to the specimens by means of liquid gel. Eventually, they were opened to observe the fracture surfaces.

3.4. Data reduction

3.4.1. Data reduction technique

Since FUMD specimens have a thermoelastic behaviour that is, at a laminate level, identical to that of a UD specimen, standard data reduction techniques [3] may be used. Since the results obtained

with the Modified Beam Theory (MBT), the Compliance calibration (CC) and the Modified Compliance calibration (MCC) are almost undistinguishable, only results obtained with MBT will be presented. Accordingly, ERR is computed as follows:

$$G_I = \frac{3P\delta}{2b(a+\Delta)}, \tag{7}$$

where P is the applied load, δ is the opening displacement, b is the specimen width and a is the delamination length. The correction Δ is determined according to [3].

3.4.2. Initiation values of G_{Ic}: insert tip vs mode I precrack

Initiation values of the critical ERR, G_{Ic}, were obtained both for the first loading phase and the second loading phase, with delamination progressing from the insert film tip and from the mode I precrack respectively, as suggested in [3].

The evaluation from the insert film tip has some advantages: the initial delamination length a_0 is known with great accuracy and it is consistent for all specimens. In addition, the insert film front is known to be straight. This reduces the experimental scatter. Conversely, during the second loading phase, the delamination length, a_0^{pc}, is slightly different for different specimens. Also, delamination is likely to have developed a curved front. This might introduce scatter in the results.

On the other hand, reliability of G_{Ic} values obtained from the insert tip is questionable: thickness, material and shape of the insert may affect the evaluation of G_{Ic} [70, 71]. If films thicker than 13 μm are used, a resin pocket may exists at the insert tip [72], which may affect results [2, 73]. Evaluation of G_{Ic} during the second loading phase, instead, avoids this problem [72].

3.4.3. Initiation values of G_{Ic}: initiation points

All initiation points defined in [3] were used to obtain G_{Ic}. The Non-Linear (NL) point was obtained fixing a threshold on the second derivative of the load displacement curves, to identify deviation from linearity. The visual onset (VIS) point was obtained by visual analysis of the digital images taken during the tests. The 5% compliance offset or maximum load (5%/MAX) point was obtained according to its definition [3]. More precisely, according to [3], the 5%/MAX value of Gc is obtained by finding the intersection of the load-deflection curve, once it has become nonlinear, with a line drawn from the origin and offset by a 5% increase in compliance from the original linear region of the load displacement. However, if the intersection occurs after the maximum load point, the maximum load is used to calculate the 5%/MAX value of Gc.

3.4.4. Propagation values of G_{Ic}

To obtain resistance curves (R-curves), G_{Ic} was evaluated also for different propagation lengths. Pictures taken during the tests were visually analysed to find those corresponding to given delamination lengths. The first point of each curve corresponds to the VIS point of the first loading phase. Subsequent

points correspond to propagation lengths measured from the insert tip.

4. Results and discussion

4.1. Force-displacement behaviour

The force-displacement plots of all tests are shown in Fig. 4. They include both loading phases and report all initiation points. The curves show a good consistency, especially for the first loading phase.

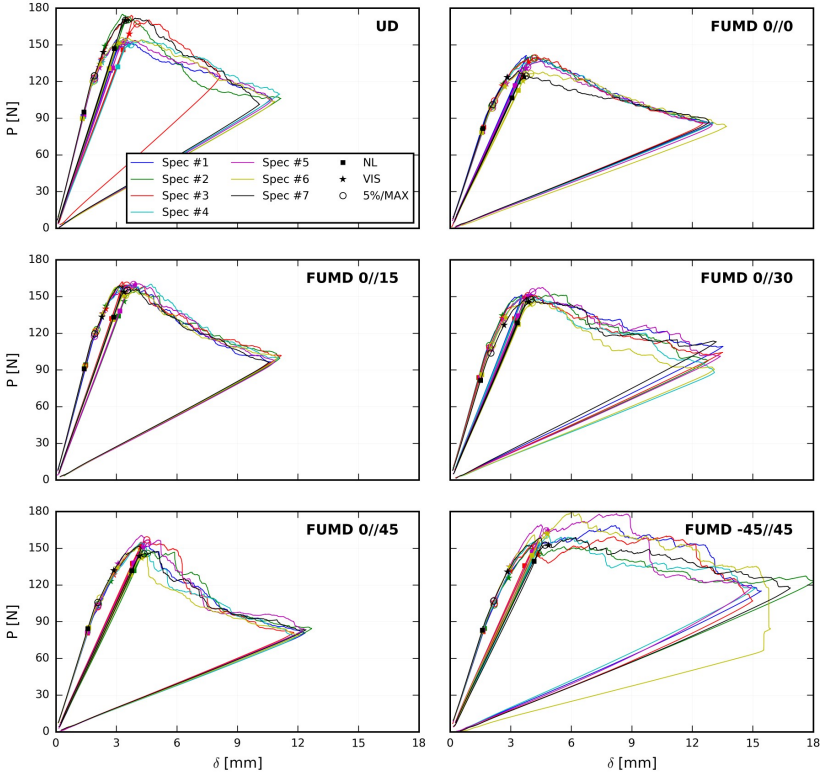

Figure 4: Force-displacement experimental curves obtained from all specimens of all sequences. Both x and y axes scales are the same for all plots.

The small scatter observed during the first unloading and the second loading phases is caused by the different delamination length, for different specimens, obtained at the end of the first loading phase, as explained in Subsection 3.4.2.

The NL point is the first observed for both loading phases. During the first phase, the 5%/MAX point is reached next, while during the second phase the 5%/MAX point is usually the last one to be reached. This may be explained by the fact that, from the insert film, delamination initially propagates

at the centre of the specimen, originating the typical thumbnail shape. Such internal propagation may be enough to increase compliance by 5% before propagation is visible on the edges of the specimen. Also the presence of a resin pocket may contribute to the initial increase in compliance in early stages of propagation. Specimens UD, FUMD 0//0, FUMD 0//15 and FUMD 0//30 show smooth softening curves, typical of stable mode I delamination propagation. On the other hand, FUMD 0//45 specimens show a faster load decrease at the beginning of the propagation, and then a smooth softening, similar to all other specimens. For FUMD -45//45 specimens, during delamination propagation, initially the force keeps increasing slightly; then, a sudden drop is observed and then force decreases. In order to understand such singular behaviour, C-scans and fracture surfaces of all FUMD -45//45 specimens were observed. Fig. 5 shows the images obtained from the C-scans (the attenuation signal, in particular) of the FUMD -45//45 specimens and of one UD specimen, for comparison. The delamination propagated

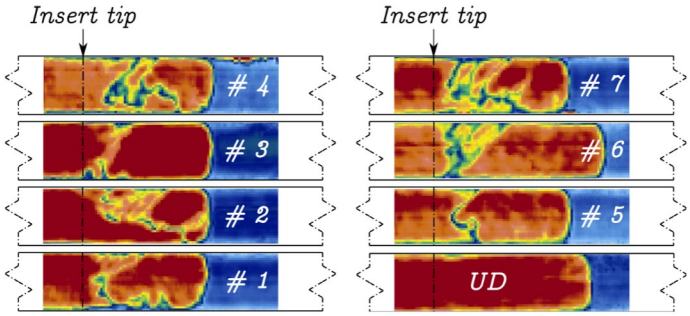

Figure 5: C-scan results of all FUMD -45//45 specimens and of a UD one.

from the left to the right. The blue regions to the right correspond to the undelaminated portion of the specimens. On the other hand, a continuous red surface, as the one observed for the UD specimen, indicates a discontinuity in the material, and hence, in this case, the delamination plane. In all the C-scans from FUMD -45//45 specimens, some irregular patterns appear. While it is not easy to draw conclusions from these images, such patterns might indicate additional damage or a delamination jump taking place. To further investigate the issue, the specimens were opened and fracture surfaces were observed. It was confirmed that in all the FUMD -45//45 specimens the delamination did not stick exclusively to its initial interface. Instead, another delamination interface appeared, toward the bottom of the stacking sequence, which is a 0//-45 interface. This is shown, for specimen # 6, in Fig. 6. It is possible to recognise a typical pattern described in other studies [12]: at first, delamination propagates on its initial plane; after few millimetres, on one edge of the specimen, delamination jumps to another interface; such jump then propagates inside the specimen following the off-axis fibres direction until the other specimen edge is reached, Fig. 6. Since delamination jump affected all FUMD -45//45 specimens, they have not been considered for subsequent analyses. Further studies are ongoing to establish if at least the initiation values of G_{Ic} could be accepted. On the other hand, both the C-scans and the observation of the fracture surfaces confirmed that a smooth propagation in the desired delamination plane was

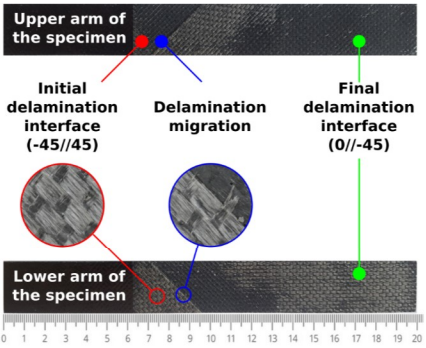

Figure 6: Fracture surfaces of specimen FUMD -45//45 number 6, confirming the occurrence of delamination jump.

obtained with all other specimens.

4.2. Initiation values of G_{Ic}

Fig. 7 reports the G_{Ic} values obtained for all the initiation points considered (NL, VIS and 5%/MAX) and for both loading phases.

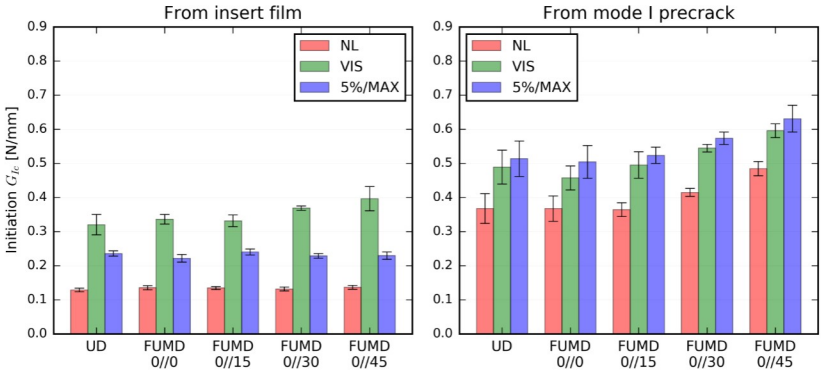

Figure 7: Initiation values of G_{Ic}.

From the insert film, values of G_{Ic} corresponding to the NL and the 5%/MAX points are independent from the delamination interface. However, as explained in subsection 3.4.2, these results may be an artefact of the resin pocket existing at the insert film tip. This seems likely, since the film adopted is 25 μm thick, thus exceeding the 13 μm limit recommended in [3]. On the other hand, the VIS values of G_{Ic} increase slightly with increasing plies mismatch angle. This might be explained by the fact that VIS points are the last to occur. While NL initiation is likely associated with delamination starting to propagate at the centre of the specimens [1], when propagation is detected visually from the specimen

side, delamination has assumed a curved shape and has propagated more in the central region of the specimens. Consequently, the effects of the resin pocket may be relevant, at most, only in a region very close to the specimens edges, and the G_{Ic} obtained should be more representative of the actual interface behaviour.

This hypothesis is corroborated by the results obtained for the delamination advancing from the mode I precrack. In this case, indeed, all G_{Ic} values obtained show a consistent increasing trend with increasing interface plies mismatch angle. In particular, the G_{Ic} values of FUMD 0//0 and FUMD 0//45 specimens are significantly different: since these two specimen types have identical global stiffness (and, being FUMD, do not have elastic couplings and thermal residual stresses), the difference may be attributed to the different orientations of interface plies. Additionally, G_{Ic} values obtained from UD and FUMD 0//0 specimens are very similar. These two specimen types share the same delamination interface, but have very different global stiffness properties. Consequently, we could postulate that interlaminar fracture toughness does not depend on global stiffness. This corroborates the hypothesis that the trend observed is not related to the global properties of the specimens, but rather it is caused by ply orientations.

Finally, values of G_{Ic} obtained from the mode I precrack should be regarded as more reliable and relevant, while those obtained from the insert tip should be regarded with caution. The differences between the two sets of data are likely explained by the effect of the thick insert film and by the build-up of transverse yarns debonding, as it will be explained later in the paper.

4.3. R-curves

Fig. 8 shows the average R-curves for all specimen types, along with the relative standard deviations.

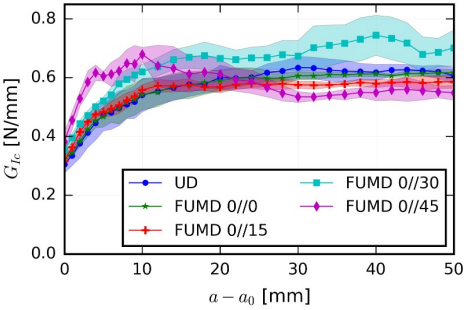

Figure 8: R-curves: average curve for all types of specimens and relative standard deviation.

Specimens UD and FUMD 0//0 have an almost identical behaviour: their R-curves start from close values, have an initial increase characterised by a similar slope and, for propagation length greater than 30 mm, both stabilize at a similar level. The scatter band is narrow for both sequences, but particularly for FUMD 0//0. These results confirm that global stiffness and stacking sequence do not affect interlaminar fracture toughness, as long as the delamination interface is the same.

Qualitatively, the behaviour of FUMD 0//15 specimens is similar to that of UD and FUMD 0//0 ones, with values of G_{Ic} that are slightly higher in the first increasing portion of the curve, and slightly lower in the stable portion.

The R-curve of sequence FUMD 0//30 presents a steeper initial increase and reaches higher values than those of the other sequences. It also has a wider scatter. For propagation length greater than 20 mm the curve does not seem to grow significantly, but shows some oscillations.

The resistance curve of sequence FUMD 0//45 shows the steepest initial increase. After a propagation of about 10 mm, however, G_{Ic} decreases and, for propagation lengths greater than 30 mm, it stabilizes to a value which is lower than those of all other sequences.

In no specimen tested did fibre-bridging occur, as confirmed by the pictures taken during the tests, see e.g. Fig. 2.

4.4. Fracture behaviour

To explain the trends of G_{Ic}, the fracture behaviour of the specimens was investigated by analysing their fracture surfaces and the pictures taken during tests.

Transverse yarn debonding was observed for all specimen types. This mechanism may occur during delamination tests of woven composites and was explained by Alif *et al.* [59, 60] and later observed also by Ozdil et al. [54, 55, 56]. Since it represents a dissipative mechanism, it contributes to the observed G_{Ic} [59]. Evidences of transverse yarns debonding for all types of specimens are shown in Fig. 9. In UD

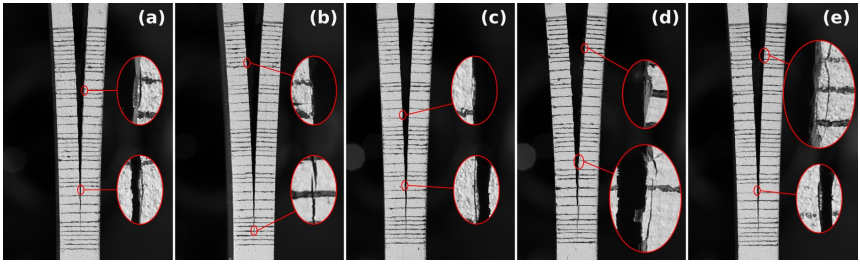

Figure 9: Evidences of transverse yarns debonding: UD (a), FUMD 0//0 (b), FUMD 0//15 (c), FUMD 0//30 (d) and FUMD 0//45 (e) specimens.

and FUMD 0//0 specimens, the phenomenon was marginal, while it became increasingly important for FUMD 0//15, FUMD 0//30 and FUMD 0//45 specimens. Similar results were reported in [54], where fracture toughness of angle-ply specimens increased with ply misalignment, due to the increasing amount of transverse yarn debonding. Results also confirm that the debonding of transverse yarns is highly dependent on the degree of constraint they experience close to the specimen edges; similar findings are reported in [60]. When UD and FUMD 0//0 specimens are considered, transverse yarns intersecting the specimens edges are only the weft yarns of the material, which make up 10% of the total fibre weight. In this situation, transverse yarns are highly constrained. In all other cases, the presence of an off-axis ply at the delamination interface implies that also warp yarns intersect the specimens edges. Furthermore, the

greater the orientation angle, the higher the number of warp yarns intersecting the edges. Consequently, a more significant transverse yarns debonding is to be expected. Hence, the transverse yarns debonding may partly explain the differences in the behaviour of the different specimen types, especially in terms of initial increase rate of G_{Ic}. Since this mechanism is not active at the very beginning of delamination and starts to build up only when delamination reaches the edges of the specimen, it is thought to contribute to the differences in G_{Ic} from the insert and from the mode I precrack, Fig. 7 and also to the increase observe in the first mm of propagation in the R-curves in Fig. 8. Nonetheless, since the material used is a plain weave composite, this mechanism is confined to an extremely narrow region close to the edges of the specimens [60].

On the other hand, the decrease in G_{Ic} in the R-curve of FUMD 0//45 specimens and the different values in the final part of the R-curves may be explained looking at the fracture surfaces of the specimens, reported in Figs. 10 and 11. Black and white regions (resin and fibres, respectively) are observed on

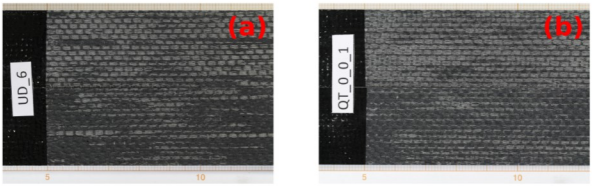

Figure 10: Example fracture surfaces: UD (a) and FUMD 0//0 (b) specimens.

all specimens, and with complementary patterns on the two fracture surfaces of each specimen. This is because separation mainly occurred at the fibre-matrix interface, rather than within the interlaminar resin layer. This indicates poor fibre-matrix adhesion properties, when compared to the matrix toughness, which often happens in glass/epoxy composites. Consequently, the interlaminar fracture toughness of the present composite is likely more influenced by the mechanical properties of the interphase (fibre-matrix interface) rather than by those of the matrix material itself. As expected, fracture surfaces of UD and FUMD 0//0 specimens look almost identical, Fig. 10, with separation randomly occurring at the fibre-matrix interface of both upper and lower plies. Fracture surfaces of FUMD 0//15 specimens are

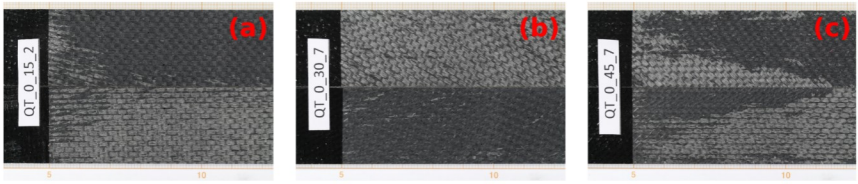

Figure 11: Example fracture surfaces: FUMD 0//15 (a), FUMD 0//30 (b) and FUMD 0//45 (c) specimens.

extremely consistent, in accordance with their force-displacement curves, Fig. 4, and with the low scatter in their R-curve, Fig. 8. Their typical aspect is that observed in Fig. 11 (a): at the very beginning both the upper (15°) and the lower plies are affected by some matrix-fibre separation, but after few millimetres, separation occurs almost entirely at the fibre-matrix interface of the 0° ply (it is noted here

that the interlaminar layer is extremely thin with respect to the arm thickness, due to the very significant ply thickness and to the high number of plies per specimen arm, and hence no effects on arms stiffness are expected). Contrarily, in FUMD 0//30 specimens separation runs almost entirely in the fibre-matrix interface of the 30° ply, Fig. 11 (b). There is one exception, represented by specimen # 6, in which some areas of separations at the 0° ply are observed. In FUMD 0//45 specimens, separation typically occurs at both fibre-matrix interfaces in the first stages of propagation, and then slowly turns most to the 0° ply fibre-matrix interface when delamination advances, as observed in Fig. 11 (c). Once again a single specimen, # 6, represents an exception: separation occurred mostly at the 0° ply for the entire propagation. These observations lead to the following conclusions. Firstly, FUMD 0//30 specimens were the only ones where separation occurred almost entirely at the fibre-matrix interface of the off-axis (30°) ply, and concurrently those yielding the highest values of propagation G_{Ic}. Conversely, UD, FUMD 0//0 and FUMD 0//15 specimens yielded lower and similar values of propagation G_{Ic} and for them separation occurred at the 0° ply fibre-matrix interface. It seems, then, that separation at the fibre-matrix interface of the off-axis plies does require higher fracture energies. This hypothesis would also explain the behaviour of FUMD 0//45 specimens: in the first stages of propagation an higher energy is required due to separation occurring mostly at the 45° ply; then energy is reduced because of separation taking place mostly at the 0° ply.

A deeper analysis, comparing fracture surfaces of single specimens to their respective R-curves corroborates the previous conclusion. In Fig. 12, R-curves of FUMD 0//30 specimens (on the left) and FUMD 0//45 specimens (on the right) have been aligned with the pictures of fracture surfaces of two representative specimens: the ones reported at the top of Fig. 12 are representative of the typical fracture behaviour of FUMD 0//30 and FUMD 0//45 specimens, respectively, while the ones at the bottom are those of the outlier specimens (specimen # 6 in both cases). The differences observed in the R-curves of the outliers specimens correlates with their different fracture surfaces. Moreover, there seems to be a strong correlation between G_{Ic} and the way separation is split between fibre-matrix interface at the off-axis and the 0° plies, as observed in Fig. 12 by reporting some relevant point of the R-curves to the fracture surfaces by means of dashed lines. Hence, the difference in G_{Ic} values at propagation may be explained by a different fracture energy required for separation at the off-axis or at the 0° plies, probably due to different fracture mechanism occurring at the micro-scale.

4.5. Specimens rotations

Besides the observation of the delamination behaviour of different interfaces, the goal of this study was to collect evidences of the suitability of FUMD specimens for delamination testing. The specimen must guarantee that the ideal kinematic of the test is respected. In a DCB test, to truly obtain pure mode I, the specimen must open in a symmetric way: its arms should rotate of the same quantity and its midplane should not rotate. While this is easily achieved with UD specimens, with MD ones this might not be the case. If the arms of the specimen are not of equal stiffness, or if couplings exist, their rotations might be different and/or the entire specimen might rotate, thus invalidating the test. According to Fig. 13, different angular quantities may be defined:

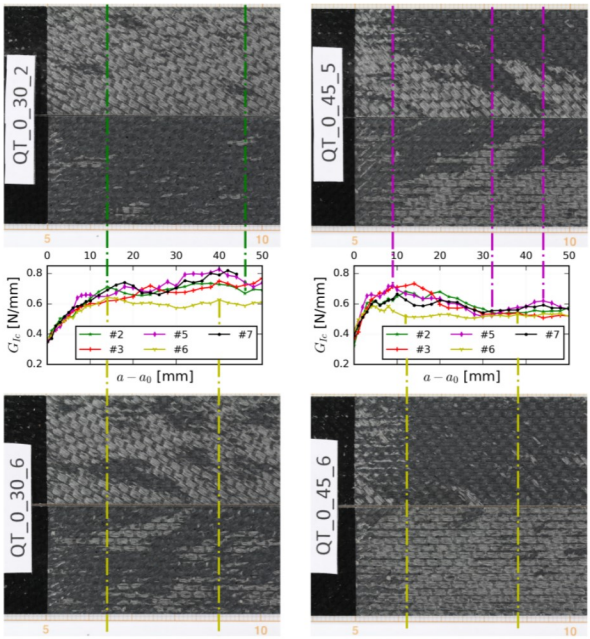

Figure 12: Comparison of R-curves with corresponding fracture surfaces for different specimens. FUMD 0//30 specimens on the left; FUMD 0//45 specimens on the right.

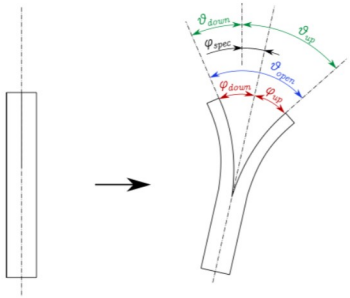

Figure 13: Definition of the different rotation angles characterising the DCB specimen during the test.

- the arm deflections φ_{down} and φ_{up} of the lower and upper arms (according to the bottom-up definition of the stacking sequences in Section 2), respectively;
- the overall opening angle of the specimen θ_{open};
- the rotation of the specimen midplane φ_{spec};
- the load points' rotations θ_{down} and θ_{up}.

The opening angle θ_{open} may be obtained as:

$$\theta_{open} = \varphi_{up} + \varphi_{down} = \theta_{up} + \theta_{down} \,. \tag{8}$$

Assuming a positive value of φ_{spec} if the rotation of the specimen is toward its upper arm:

$$\theta_{up} = \varphi_{up} + \varphi_{spec} \,, \tag{9}$$

$$\theta_{down} = \varphi_{down} - \varphi_{spec} \,. \tag{10}$$

If the specimen is symmetric from an elastic point of view, then it is expected that:

$$\varphi_{spec} = 0 \,, \tag{11}$$

$$\varphi_{up} = \varphi_{down} = \theta_{down} = \theta_{up} = \theta \,, \tag{12}$$

$$\theta_{open} = 2\theta \,. \tag{13}$$

In this study, both UD and FUMD specimens are theoretically expected to satisfy in first approximation the relationships in Eqs. (11)-(13). Hence, the load points rotations θ_{down} and θ_{up}, were measured by means of inclinometers throughout the whole test and for all specimens. To evaluate the behaviour of FUMD delamination specimens and to compare it to that of UD ones, the quantity $\Delta\bar{\theta}$ was defined:

$$\Delta\bar{\theta} = \frac{\theta_{up} - \theta_{down}}{\theta_{up} + \theta_{down}} \cdot 100 \,. \tag{14}$$

This quantity represents the difference of the load point rotations as a percentage of the total opening angle of the specimen. While ideally $\Delta\bar{\theta}$ should be zero, small deviations are expected to occur, even for UD specimens, due to experimental uncertainties (thickness variations of the arms, specimens placement at the beginning of the test, etc.). It is important that deviations of FUMD specimen be comparable with thos of UD ones. Four representative points in the load displacement curves have been chosen to evaluate $\Delta\bar{\theta}$:

1. Half of Maximum Load Point (HMLP);
2. Maximum Load Point (MLP);
3. Reduced Stiffness Point (RSP): the point, during delamination propagation, at which the specimen stiffness is reduced by 50%;
4. Maximum Opening Point (MOP).

For illustration purposes, such points are shown in Fig. 14 (a), on the force-displacement curve of one of the specimens. The average values of $\Delta\bar{\theta}$ for all sets of specimens have been computed and are shown in Fig. 14, along with their standard deviation.

A first general observation is that average values of $\Delta\bar{\theta}$ are very small for all specimen types, and never exceed 5% of the total specimen opening angles.

Considering UD specimens, they show non-null average values of $\Delta\bar{\theta}$. However, the scatter interval defined by the standard deviation is wider than the average value and thus contain the zero. This means that, in general, there was no one arm (upper or lower) that consistently rotated more than the other

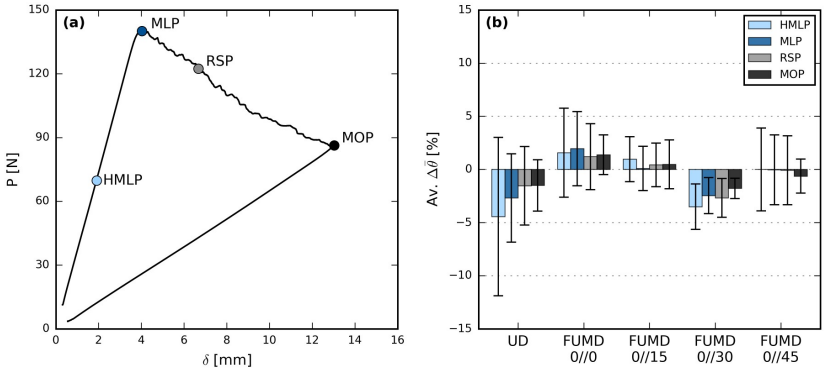

Figure 14: Illustration of experimental points used to evaluate $\Delta\bar{\theta}$ (a) and mean values and standard deviations obtained for each set of specimens (b).

one. Especially considering the symmetry of UD specimens, the small deviations observed are likely to be due to random variability of manufacturing and test conditions.

Most importantly, average values obtained with FUMD specimens are comparable to, or even lower than, those of UD specimens. Additionally, the standard deviation once again oscillates around zero, confirming the generally symmetric behaviour of the specimens. FUMD 0//30 specimens represent an exception in that their $\Delta\bar{\theta}$ values tend toward the negative side (greater rotation of the lower arm) and their standard deviation do not cross the zero. However, such values remain extremely small and even included within the scatter band of UD specimens.

While further studies using more advanced techniques (such as Digital Image Correlation) could give a more detailed and complete picture, these observations seem to corroborate the suitability of FUMD sequences for delamination testing of MD specimens.

4.6. Delamination front analysis via ultrasonic C-scans

One of the most important feature of standard UD specimens is the capability to produce a delamination front as straight and symmetric as possible. This is the consequence of an appropriate mechanical behaviour of the specimen throughout the test. While this is extremely important in order to perform good tests and correctly reduce data, it also becomes very difficult to be obtained when using MD specimens. It was shown by finite element analysis in [44] that FUMD DCB specimens approach closely the optimal ERR modal partition obtainable with standard UD specimens. The goal of this study was therefore to verify if also delamination fronts obtained with FUMD specimens are satisfactorily similar to those of UD specimens, since such similarity would represent an actual experimental evidence of validation of the concept. Therefore, ultrasonic C-scans of the unloaded specimens were performed after the tests. Such scan allow to observe discontinuities within the material, thus being particularly suited to detect the presence of delaminations. Fig. 15 reports representative C-scans for all specimen types. The fronts

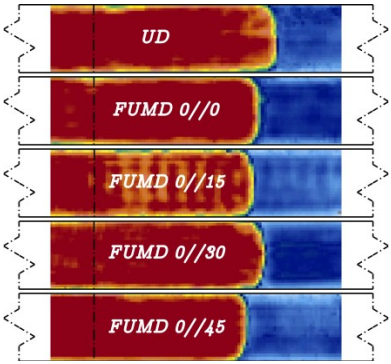

Figure 15: Representative C-scans for all sequences adopted. In this view, delamination propagated from the left to the right. The dashed line superposed to the C-scan images is the location of the insert tip.

obtained with FUMD sequences appear symmetric and with a mild curvature, comparable to that of UD ones. C-scan images have been post-processed up to the attainment of a one-pixel-thick delamination front, with the process shown in Fig. 16, for one of the FUMD 0//30 specimens. To quantitatively

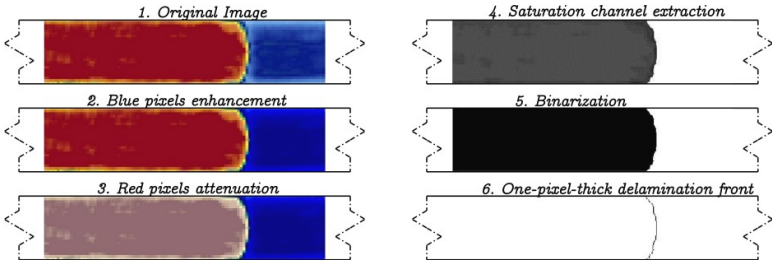

Figure 16: Example of C-scan images processing steps, from the original image to the one-pixel-thick delamination front.

evaluate the curvature and the asymmetry of the delamination front, two parameters were defined. The first one, β gives an estimation of the curvature of the front, and is defined as:

$$\beta = \frac{|x^{max} - x^{av}|}{b} . \tag{15}$$

In Eq (15), $|x^{max} - x^{av}|$ is the distance between the point of farthest propagation and the average line of the delamination front (note that this quantity does not depend on the x origin), and b is the specimen width. Parameter β would be 0 only for a perfectly straight delamination front, while it would be 1 if the tip of the delamination front lies one specimen width ahead of the average line of the front itself. The second parameter, γ, quantifies the asymmetry of the front, and is defined as follows:

$$\gamma = \frac{\sum_{y} |x^{(y)} - x^{(-y)}|}{b * n_y} . \tag{16}$$

In Eq. (16), $|x^{(y)} - x^{(-y)}|$ is the difference in propagation length between two specular points(with respect to the specimen longitudinal symmetry plane) of the delamination front; such quantity is summed for all couples of corresponding pixels and then normalized by the number of couples (n_y) and the specimen width. Hence, γ represents an average measure of propagation asymmetry of specular front pixels relative to the specimen width. This parameter would be equal to 0 only if the delamination front is perfectly symmetric, while it would be 1 if, on average, each couple of corresponding front pixels has a difference in propagation length equal to the specimen width. Both β and γ have been evaluated for all specimens. The average and standard deviation of the results over each set of specimens are reported in Fig. 17.

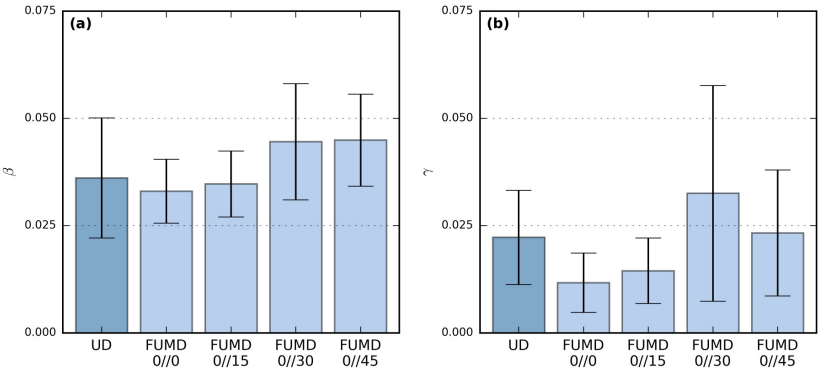

Figure 17: Mean values and standard deviation for the parameters β (a), quantifying delamination front curvature, and γ (b), quantifying delamination front asymmetry.

Values of β found, Fig. 17 (a), are extremely small, confirming that fairly straight fronts have been obtained. Moreover, no trend in the data for the different layups may be clearly identified, since differences between data from FUMD specimens and UD ones are so small that they fall within the experimental scatter. This confirms that curvature of delamination fronts obtained with FUMD specimens is comparable to that obtained with UD ones.

Similarly, it appears that no correlation exists between delamination front asymmetry and the interface plies mismatch angle, Fig. 17 (b). Values of γ are extremely small for all layups, with the only exception of sequence FUMD 0//30, which also shows a significantly wider scatter band. Indeed, few FUMD 0//30 specimens show a more asymmetric delamination front. At present, no explanation has been found for this inconsistent behaviour, but additional analyses will be performed. Other FUMD specimens are seen to perform as well as UD ones, with the small asymmetry measured likely related to material and experimental variability rather than to the stacking sequence. This supports the expected uncoupled behaviour of FUMD specimens, which leads to avoid undesired delamination front asymmetries.

5. Summary, conclusions and perspectives

In this paper, an experimental study to assess the suitability of FUMD specimens for delamination tests was presented. Five different types of FUMD specimens, having different delamination interfaces, were designed. A glass/epoxy UD-fabric material was used to reduce the likelihood of delamination jump. The specimens were tested under pure mode I delamination, according to standard procedures. For comparison purposes, also standard UD specimens of the same material were tested. Four out of five FUMD specimen types did not experience any delamination jump, and the propagation was smooth and continuous in the initial delamination plane, as confirmed by C-scan images and fracture surfaces observation.

As far as critical ERR, G_{Ic}, is concerned, no dependence on the global stiffness of the specimens was observed. On the other hand, increasing interface plies mismatch angles led to increased initiation G_{Ic}. No fibre bridging was observed, and the values of G_{Ic} during propagation were different for different plies mismatch angles. In particular, values of G_{Ic} were influenced by the amount of transverse yarns debonding and the different fracture behaviour of the specimens. Of course, further research, involving different materials and interfaces, is required to clearly understand how orientations of plies affect the interlaminar fracture toughness.

Nonetheless, this study gives a first indication that FUMD specimens are suitable candidates for obtaining optimal delamination testing conditions. The measurement of the rotations of the loading points during the tests showed that FUMD specimens have a behaviour in line with that of UD ones. Furthermore, results in terms of delamination front curvature and asymmetry, derived from C-scan images, show that FUMD specimens produce delamination fronts that are comparable to those observed in UD specimens.

In conclusion, since FUMD sequences allow the design of specimens with different delamination interfaces and mechanical properties, they may be useful to study almost any aspect of delamination in multidirectional laminates, from migration to fracture toughness evaluation. So the use of FUMD sequence could provide a general foundation to obtain more consistent, repeatable and clear results even from different studies. Despite a lot of work remains to be done to confirm such possibility, FUMD sequence are believed to represent a valid candidate for a future standard for delamination testing of multidirectional interfaces.

6. Acknowledgements

The first author is grateful to region Nouvelle Aquitaine for funding this research through the SMART-COMPOSITE project. Colleagues F. Ricci, E. Monaco and N. D. Boffa from University of Naples Federico II are kindly acknowledged for performing the ultrasonic C-scan of the specimens.

Data availability

The raw and processed data required to reproduce these findings cannot be shared at this time as the data also forms part of an ongoing study.

References

[1] P. Davies, B. R. K. Blackman, A. J. Brunner, Standard test methods for delamination resistance of composite materials: Current status, Applied Composite Materials 5 (6) (1998) 345–364. doi:10.1023/A:1008869811626.
URL https://doi.org/10.1023/A:1008869811626

[2] T. O'Brien, Interlaminar fracture toughness: the long and winding road to standardization, Composites Part B: Engineering 29 (1) (1998) 57 – 62. doi:https://doi.org/10.1016/S1359-8368(97)00013-9.
URL http://www.sciencedirect.com/science/article/pii/S1359836897000139

[3] ASTM D5528-13, Standard Test Method for Mode I Interlaminar Fracture Toughness of Unidirectional Fiber-Reinforced Polymer Matrix Composites, Tech. rep., ASTM International, West Conshohocken, PA (2013).
URL www.astm.org

[4] ASTM D7905/D7905M-14, Standard Test Method for Determination of the Mode II Interlaminar Fracture Toughness of Unidirectional Fiber-Reinforced Polymer Matrix Composites, Tech. rep., ASTM International, West Conshohocken, PA (2014).
URL www.astm.org

[5] ASTM D6671 / D6671M-13e1, Standard Test Method for Mixed Mode I-Mode II Interlaminar Fracture Toughness of Unidirectional Fiber Reinforced Polymer Matrix Composites, Tech. rep., ASTM International, West Conshohocken, PA (2013).
URL www.astm.org

[6] S. Lee, An Edge Crack Torsion Method for Mode III Delamination Fracture Testing, Journal of Composites Technology & Research 15 (3) (1993) 193–201.
URL https://doi.org/10.1520/CTR10369J

[7] M. W. Czabaj, B. D. Davidson, J. G. Ratcliffe, A modified edge crack torsion test for measurement of mode III fracture toughness of laminated tape composites, in: 31st Annual Technical Conference of the American Society for Composites, ASC 2016, DEStech Publications Inc., 2016.
URL https://ntrs.nasa.gov/search.jsp?R=20160012238

[8] C. Audd, B. D. Davidson, J. G. Ratcliffe, M. W. Czabaj, Reexamination of the edge crack torsion test for determining the mode III delamination toughness of laminated composites, Engineering Fracture Mechanics 215 (2019) 138 – 150. doi:https://doi.org/10.1016/j.engfracmech.2019.05.007.
URL http://www.sciencedirect.com/science/article/pii/S0013794419300396

[9] A. Tabiei, W. Zhang, Composite Laminate Delamination Simulation and Experiment: A Review of Recent Development, Applied Mechanics Reviews 70 (3), 030801. doi:10.1115/1.4040448.
URL https://doi.org/10.1115/1.4040448

[10] J. Andersons, M. König, Dependence of fracture toughness of composite laminates on interface ply orientations and delamination growth direction, Composites Science and Technology 64 (13-14) (2004) 2139–2152. doi:10.1016/j.compscitech.2004.03.007.

[11] M. Charalambides, J. Williams, Mode I delamination of angle-ply epoxy/glass-fibre laminates exhibiting permanent deformation during fracture, Composites Science and Technology 50 (2) (1994) 187 – 196. doi:https://doi.org/10.1016/0266-3538(94)90140-6.
URL http://www.sciencedirect.com/science/article/pii/0266353894901406

[12] J. Tao, C. T. Sun, Influence of ply orientation on delamination in composite laminates, Journal of Composite Materials 32 (21) (1998) 1933–1947. arXiv:https://doi.org/10.1177/002199839803202103, doi:10.1177/002199839803202103.
URL https://doi.org/10.1177/002199839803202103

[13] A. Laksimi, A. A. Benyahia, M. Benzeggagh, X. Gong, Initiation and bifurcation mechanisms of cracks in multi-directional laminates, Composites Science and Technology 60 (4) (2000) 597 – 604. doi:https://doi.org/10.1016/S0266-3538(99)00179-7.
URL http://www.sciencedirect.com/science/article/pii/S0266353899001797

[14] J. Schön, T. Nyman, A. Blom, H. Ansell, A numerical and experimental investigation of delamination behaviour in the DCB specimen, Composites Science and Technology 60 (2) (2000) 173 – 184. doi:https://doi.org/10.1016/S0266-3538(99)00113-X.
URL http://www.sciencedirect.com/science/article/pii/S026635389900113X

[15] A. de Morais, M. de Moura, A. Marques, P. de Castro, Mode I interlaminar fracture of carbon/epoxy cross-ply composites, Composites Science and Technology 62 (5) (2002) 679 – 686. doi:https://doi.org/10.1016/S0266-3538(01)00223-8.
URL http://www.sciencedirect.com/science/article/pii/S0266353801002238

[16] T. Sebaey, N. Blanco, J. Costa, C. Lopes, Characterization of crack propagation in mode I delamination of multidirectional CFRP laminates, Composites Science and Technology 72 (11) (2012) 1251 – 1256. doi:https://doi.org/10.1016/j.compscitech.2012.04.011.
URL http://www.sciencedirect.com/science/article/pii/S0266353812001662

[17] C. Blondeau, G. Pappas, J. Botsis, Influence of ply-angle on fracture in antisymmetric interfaces of CFRP laminates, Composite Structures 216 (2019) 464 – 476. doi:https://doi.org/10.1016/j.compstruct.2019.03.004.
URL http://www.sciencedirect.com/science/article/pii/S0263822319303307

[18] C. Canturri, E. S. Greenhalgh, S. T. Pinho, The relationship between mixed-mode II/III delamination and delamination migration in composite laminates, Composites Science and Technology 105 (2014) 102 – 109. doi:https://doi.org/10.1016/j.compscitech.2014.10.001.
URL http://www.sciencedirect.com/science/article/pii/S0266353814003558

[19] B. Chen, T. Tay, S. Pinho, V. Tan, Modelling delamination migration in angle-ply laminates, Composites Science and Technology 142 (2017) 145 – 155. doi:https://doi.org/10.1016/j.compscitech.2017.02.010.
URL http://www.sciencedirect.com/science/article/pii/S0266353816308818

[20] J. Barnes, G. Byerly, The formation of residual stresses in laminated thermoplastic composites, Composites Science and Technology 51 (4) (1994) 479 – 494. doi:https://doi.org/10.1016/0266-3538(94)90081-7.
URL http://www.sciencedirect.com/science/article/pii/0266353894900817

[21] T. Sebaey, N. Blanco, C. Lopes, J. Costa, Numerical investigation to prevent crack jumping in double cantilever beam tests of multidirectional composite laminates, Composites Science and Technology 71 (13) (2011) 1587–1592.

[22] J. A. Nairn, Fracture Mechanics of Composites With Residual Thermal Stresses, Journal of Applied Mechanics 64 (4) (1997) 804–810. arXiv:https://asmedigitalcollection.asme.org/appliedmechanics/article-pdf/64/4/804/4727361/804_1.pdf, doi:10.1115/1.2788985.
URL https://doi.org/10.1115/1.2788985

[23] J. A. Nairn, Energy release rate analysis for adhesive and laminate double cantilever beam specimens emphasizing the effect of residual stresses, International Journal of Adhesion and Adhesives 20 (1) (2000) 59 – 70. doi:https://doi.org/10.1016/S0143-7496(99)00016-0.
URL http://www.sciencedirect.com/science/article/pii/S0143749699000160

[24] J. A. Nairn, On the calculation of energy release rates for cracked laminates with residual stresses, International Journal of Fracture 139 (2) (2006) 267. doi:10.1007/s10704-006-0044-0.
URL https://doi.org/10.1007/s10704-006-0044-0

[25] T. Yokozeki, T. Ogasawara, T. Aoki, Correction method for evaluation of interfacial fracture toughness of DCB, ENF and MMB specimens with residual thermal stresses, Composites Science and Technology 68 (3-4) (2008) 760–767. doi:10.1016/j.compscitech.2007.08.025.

[26] R. Krueger, Virtual crack closure technique: History, approach, and applications, Applied Mechanics Reviews 57 (2) (2004) 109. doi:10.1115/1.1595677.
URL http://appliedmechanicsreviews.asmedigitalcollection.asme.org/article.aspx?articleid=1397949

[27] R. Krueger, K. N. Shivakumar, I. S. Raju, Fracture Mechanics Analyses for Interface Crack Problems - A Review, 54th AIAA/ASME/ASCE/AHS/ASC Structures, Structural Dynamics, and Materials Conferencedoi:10.2514/6.2013-1476.
URL http://arc.aiaa.org/doi/10.2514/6.2013-1476

[28] T. Kalbermatten, R. Jäggi, P. FLüeler, H. Kausch, P. Davies, Microfocus radiography studies during mode I interlaminar fracture tests on composites, Journal of Materials Science Letters 11 (9) (1992) 543–546. doi:https://doi.org/10.1007/BF00728603.

[29] S. Samborski, Prediction of delamination front's advancement direction in the CFRP laminates with mechanical couplings subjected to different fracture toughness tests, Composite Structures 202 (2018) 643 – 650, special issue dedicated to Ian Marshall. doi:https://doi.org/10.1016/j.compstruct.2018.03.045.
URL http://www.sciencedirect.com/science/article/pii/S0263822318303957

[30] L. Carreras, B. Bak, A. Turon, J. Renart, E. Lindgaard, Point-wise evaluation of the growth driving direction for arbitrarily shaped delamination fronts using cohesive elements, European Journal of Mechanics - A/Solids 72 (Int. J. Numer. Meth. Eng. 50 2001) (2018) 464–482. doi:10.1016/j.euromechsol.2018.05.006.
URL https://app.dimensions.ai/details/publication/pub.1104044548

[31] B. Davidson, R. Schapery, Effect of finite width on deflection and energy release rate of an orthotropic double cantilever specimen, Journal of Composite Materials 22 (7) (1988) 640–656. arXiv:https://doi.org/10.1177/002199838802200704, doi:10.1177/002199838802200704.
URL https://doi.org/10.1177/002199838802200704

[32] B. Davidson, An analytical investigation of delamination front curvature in double cantilever beam specimens, Journal of Composite Materials 24 (11) (1990) 1124–1137. arXiv:https://doi.org/10.1177/002199839002401101, doi:10.1177/002199839002401101.
URL https://doi.org/10.1177/002199839002401101

[33] C. Sun, S. Zheng, Delamination characteristics of double-cantilever beam and end-notched flexure composite specimens, Composites Science and Technology 56 (4) (1996) 451 – 459. doi:https://doi.org/10.1016/0266-3538(96)00001-2.
URL http://www.sciencedirect.com/science/article/pii/0266353896000012

[34] B. Davidson, R. Krüger, M. König, Effect of stacking sequence on energy release rate distributions in multidirectional dcb and enf specimens, Engineering Fracture Mechanics 55 (4) (1996) 557 – 569. doi:https://doi.org/10.1016/S0013-7944(96)00037-9.
URL http://www.sciencedirect.com/science/article/pii/S0013794496000379

[35] S. Samborski, Numerical analysis of the DCB test configuration applicability to mechanically coupled Fiber Reinforced Laminated Composite beams, Composite Structures 152 (Supplement C) (2016) 477 – 487. doi:https://doi.org/10.1016/j.compstruct.2016.05.060.
URL http://www.sciencedirect.com/science/article/pii/S0263822316305414

[36] Fibre-reinforced plastic composites — Determination of mode I interlaminar fracture toughness, GIC, for unidirectionally reinforced materials, Standard, International Organization for Standardization (Mar. 2001).

[37] B. D. Davidson, R. Kruger, M. König, Three dimensional analysis and resulting design recommendations for unidirectional and multidirectional end-notched flexure tests, Journal of Composite Materials 29 (16) (1995) 2108–2133. arXiv:https://doi.org/10.1177/002199839502901602,

doi:10.1177/002199839502901602.
URL https://doi.org/10.1177/002199839502901602

[38] B. D. Davidson, S. J. Gharibian, L. Yu, Evaluation of energy release rate-based approaches for predicting delamination growth in laminated composites, International Journal of Fracture 105 (4) (2000) 343–365. doi:10.1023/A:1007647226760.

[39] B. D. Davidson, R. D. Bialaszewski, S. S. Sainath, A non-classical, energy release rate based approach for predicting delamination growth in graphite reinforced laminated polymeric composites, Composites Science and Technology 66 (10) (2006) 1479–1496. doi:10.1016/j.compscitech.2004.10.031.

[40] P. Vannucci, G. Verchery, A special class of uncoupled and quasi-homogeneous laminates, Composites Science and Technology 61 (10) (2001) 1465 – 1473. doi:http://dx.doi.org/10.1016/S0266-3538(01)00039-2.
URL http://www.sciencedirect.com/science/article/pii/S0266353801000392

[41] X. Gong, A. Hurez, G. Verchery, On the determination of delamination toughness by using multidirectional DCB specimens, Polymer Testing 29 (6) (2010) 658 – 666. doi:https://doi.org/10.1016/j.polymertesting.2010.04.007.
URL http://www.sciencedirect.com/science/article/pii/S0142941810000747

[42] M. M. Rehan, J. Rousseau, X. Gong, L. Guillaumat, J. Ali, Effects of fiber orientation of adjacent plies on the mode I crack propagation in a carbon-epoxy laminates, Procedia Engineering 10 (Supplement C) (2011) 3179 – 3184, 11th International Conference on the Mechanical Behavior of Materials (ICM11). doi:https://doi.org/10.1016/j.proeng.2011.04.525.
URL http://www.sciencedirect.com/science/article/pii/S1877705811007132

[43] M. B. M. Rehan, J. Rousseau, S. Fontaine, X. Gong, Experimental study of the influence of ply orientation on DCB mode-I delamination behavior by using multidirectional fully isotropic carbon/epoxy laminates, Composite Structures 161 (Supplement C) (2017) 1 – 7. doi:https://doi.org/10.1016/j.compstruct.2016.11.036.
URL http://www.sciencedirect.com/science/article/pii/S0263822316307061

[44] T. Garulli, A. Catapano, D. Fanteria, J. Jumel, E. Martin, Design and finite element assessment of fully uncoupled multi-directional layups for delamination tests, Journal of Composite Materials 0 (0) (0) 0021998319868293. arXiv:https://doi.org/10.1177/0021998319868293, doi:10.1177/0021998319868293.
URL https://doi.org/10.1177/0021998319868293

[45] T. Garulli, A. Catapano, M. Montemurro, J. Jumel, D. Fanteria, Quasi-trivial solutions for uncoupled, homogeneous and quasi-homogeneous laminates with high number of plies, in: R. Owen, de Borst, Pearce (Eds.), ECCM VI, International Center for Numerical Methods in Engineering (CIMNE), 2018, pp. 255–265.

[46] T. Garulli, A. Catapano, M. Montemurro, J. Jumel, D. Fanteria, Quasi-trivial stacking sequences for the design of thick laminates, Composite Structures 200 (2018) 614 – 623. doi:https://doi.org/10.1016/j.compstruct.2018.05.120.
URL http://www.sciencedirect.com/science/article/pii/S0263822318309565

[47] E. J. Barbero, Introduction to Composite Materials Design, CRC press, 2017.

[48] A. B. De Morais, M. F. De Moura, J. P. Gonçalves, P. P. Camanho, Analysis of crack propagation in double cantilever beam tests of multidirectional laminates, Mechanics of Materials 35 (7) (2003) 641–652. doi:10.1016/S0167-6636(02)00289-2.

[49] R. Olsson, J. Thesken, F. Brandt, N. Jönsson, S. Nilsson, Investigations of delamination criticality and the transferability of growth criteria, Composite Structures 36 (3) (1996) 221 – 247. doi:https://doi.org/10.1016/S0263-8223(96)00079-7.
URL http://www.sciencedirect.com/science/article/pii/S0263822396000797

[50] L. Yong, L. Shunling, X. Jun, T. Jie, Study on the mode I interlaminar fracture toughness of multidirectional laminates, in: M. L. Scott (Ed.), Elementary particle theory, Woodhead Publishing Limited, 1997, pp. 431–437.

[51] J. H. Hwang, C. S. Lee, W. Hwang, Effect of crack propagation directions on the interlaminar fracture toughness of carbon/epoxy composite materials, Applied Composite Materials 8 (6) (2001) 411–433. doi:10.1023/A:1012663722334.
URL https://doi.org/10.1023/A:1012663722334

[52] P. Prombut, L. Michel, F. Lachaud, J. Barrau, Delamination of multidirectional composite laminates at $0/\theta$ ply interfaces, Engineering Fracture Mechanics 73 (16) (2006) 2427 – 2442, fracture of Polymers, Composites and Adhesives. doi:https://doi.org/10.1016/j.engfracmech.2006.05.013.
URL http://www.sciencedirect.com/science/article/pii/S0013794406001792

[53] K. Dadej, J. Bieniaś, B. Surowska, Interlaminar cracking resistance of nonhomogeneous composite beams, Composites Theory and Practice 17 (2017) 3–2017.

[54] F. Ozdil, L. Carlsson, P. Davies, Beam analysis of angle-ply laminate end-notched flexure specimens, Composites Science and Technology 58 (12) (1998) 1929 – 1938. doi:https://doi.org/10.1016/S0266-3538(98)00018-9.
URL http://www.sciencedirect.com/science/article/pii/S0266353898000189

[55] F. Ozdil, L. Carlsson, Beam analysis of angle-ply laminate mixed-mode bending specimens, Composites Science and Technology 59 (6) (1999) 937 – 945. doi:https://doi.org/10.1016/S0266-3538(98)00128-6.
URL http://www.sciencedirect.com/science/article/pii/S0266353898001286

[56] F. Ozdil, L. Carlsson, Beam analysis of angle-ply laminate DCB specimens, Composites Science and Technology 59 (2) (1999) 305 – 315. doi:https://doi.org/10.1016/S0266-3538(98)00069-4.
URL http://www.sciencedirect.com/science/article/pii/S0266353898000694

[57] D. Fanteria, L. Lazzeri, E. Panettieri, U. Mariani, M. Rigamonti, Experimental characterization of the interlaminar fracture toughness of a woven and a unidirectional carbon/epoxy composite, Composites Science and Technology 142 (2017) 20 – 29. doi:https://doi.org/10.1016/j.compscitech.2017.01.028.
URL http://www.sciencedirect.com/science/article/pii/S026635381631987X

[58] M. Kotaki, H. Hamada, Effect of interfacial properties and weave structure on mode I interlaminar fracture behaviour of glass satin woven fabric composites, Composites Part A: Applied Science and Manufacturing 28 (3) (1997) 257 – 266. doi:https://doi.org/10.1016/S1359-835X(96)00121-2.
URL http://www.sciencedirect.com/science/article/pii/S1359835X96001212

[59] N. Alif, L. A. Carlsson, J. W. Gillespie, Mode I, mode II, and mixed mode interlaminar fracture of woven fabric carbon/epoxy, in: S. Hooper (Ed.), Composite Materials: Testing and Design, Thirteenth Volume, Vol. 13, ASTM International, West Conshohocken, PA, 1997, pp. 82–106.

[60] N. Alif, L. A. Carlsson, L. Boogh, The effect of weave pattern and crack propagation direction on mode I delamination resistance of woven glass and carbon composites, Composites Part B: Engineering 29 (5) (1998) 603 – 611. doi:https://doi.org/10.1016/S1359-8368(98)00014-6.
URL http://www.sciencedirect.com/science/article/pii/S1359836898000146

[61] P. Suppakul, S. Bandyopadhyay, The effect of weave pattern on the mode-I interlaminar fracture energy of e-glass/vinyl ester composites, Composites Science and Technology 62 (5) (2002) 709 – 717. doi:https://doi.org/10.1016/S0266-3538(01)00220-2.
URL http://www.sciencedirect.com/science/article/pii/S0266353801002202

[62] Y. Wang, D. Zhao, Characterization of interlaminar fracture behaviour of woven fabric reinforced polymeric composites, Composites 26 (2) (1995) 115 – 124. doi:https://doi.org/10.1016/0010-4361(95)90411-R.
URL http://www.sciencedirect.com/science/article/pii/001043619590411R

[63] J.-K. Kim, M.-L. Sham, Impact and delamination failure of woven-fabric composites, Composites Science and Technology 60 (5) (2000) 745 – 761. doi:https://doi.org/10.1016/S0266-3538(99)00166-9.
URL http://www.sciencedirect.com/science/article/pii/S0266353899001669

[64] ASTM D3039 / D3039M - 17, Standard Test Method for Tensile Properties of Polymer Matrix Composite Materials, Tech. rep., ASTM International, West Conshohocken, PA (2017).
URL www.astm.org

[65] ASTM D3518 / D3518M - 18, Standard Test Method for In-Plane Shear Response of Polymer Matrix Composite Materials by Tensile Test of a ±45 ° Laminate, Tech. rep., ASTM International, West Conshohocken, PA (2018).
URL www.astm.org

[66] ASTM D7264 / D7264M - 15, Standard Test Method for Flexural Properties of Polymer Matrix Composite Materials, Tech. rep., ASTM International, West Conshohocken, PA (2015).
URL www.astm.org

[67] C. Meola, S. Boccardi, G. Carlomagno, N. Boffa, E. Monaco, F. Ricci, Nondestructive evaluation of carbon fibre reinforced composites with infrared thermography and ultrasonics, Composite Structures 134 (2015) 845 – 853. doi:https://doi.org/10.1016/j.compstruct.2015.08.119.
URL http://www.sciencedirect.com/science/article/pii/S0263822315008156

[68] S. Boccardi, N. D. Boffa, G. M. Carlomagno, L. Maio, C. Meola, F. Ricci, Infrared thermography and ultrasonics to evaluate composite materials for aeronautical applications, Journal of Physics: Conference Series 658 (2015) 012007. doi:10.1088/1742-6596/658/1/012007.

[69] L. Maio, V. Memmolo, S. Boccardi, C. Meola, F. Ricci, N. Boffa, E. Monaco, Ultrasonic and IR thermographic detection of a defect in a multilayered composite plate, Procedia Engineering 167 (2016) 71–79. doi:10.1016/j.proeng.2016.11.671.

[70] M. Todo, P.-Y. Jar, Study of mode-I interlaminar crack growth in DCB specimens of fibre-reinforced composites, Composites Science and Technology 58 (1) (1998) 105 – 118. doi:https://doi.org/10.1016/S0266-3538(97)00102-4.
URL http://www.sciencedirect.com/science/article/pii/S0266353897001024

[71] D. Stevanovic, P.-Y. Jar, S. Kalyanasundaram, A. Lowe, On crack-initiation conditions for mode I and mode II delamination testing of composite materials, Composites Science and Technology 60 (9) (2000) 1879 – 1887. doi:https://doi.org/10.1016/S0266-3538(00)00080-4.
URL http://www.sciencedirect.com/science/article/pii/S0266353800000804

[72] M. Hojo, K. Kageyama, K. Tanaka, Prestandardization study on mode I interlaminar fracture toughness test for CFRP in Japan, Composites 26 (4) (1995) 243–255. doi:10.1016/0010-4361(95)93668-A.

[73] A. Brunner, B. Blackman, P. Davies, A status report on delamination resistance testing of polymer–matrix composites, Engineering Fracture Mechanics 75 (9) (2008) 2779 – 2794. doi:https://doi.org/10.1016/j.engfracmech.2007.03.012.
URL http://www.sciencedirect.com/science/article/pii/S0013794407001208

Fully-**U**ncoupled
Multi- **D**irectional
(**FUMD**)

vs.

Uni-**D**irectional
(**UD**)

Mode I delamination tests

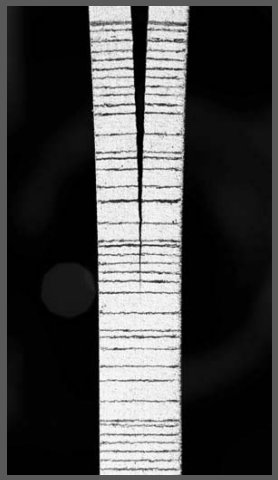

Delamination fronts

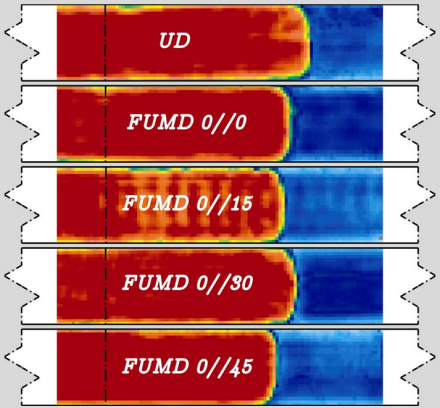

Interlaminar fracture toughness